Available online at www.sciencedirect.com
SCIENCE DIRECT®
International Journal of Heat and Mass Transfer 47 (2004) 947–958
International Journal of HEAT and MASS TRANSFER
www.elsevier.com/locate/ijhmt

An experimental study on combustion characteristics of flames in a coaxial flow with a stagnation point

Shuhn-Shyurng Hou [a,*], Shuhn-Shing Yang [b], Ta-Hui Lin [b]

[a] Department of Mechanical Engineering, Kun Shan University of Technology, Tainan 71003, Taiwan, ROC
[b] Department of Mechanical Engineering, National Cheng Kung University, Tainan 70101, Taiwan, ROC

Received 25 November 2002; received in revised form 18 August 2003

Abstract

By using a stagnation-point coaxial flow generated by a lower coaxial burner and an upper quartz plate, an inner (or outer) premixed flame influenced by outer (or inner) oxygen content is experimentally developed to simulate and study double-flame burning structures modified by interactions of flamelets in turbulent combustible flows. In the experiments, fuel–air and oxygen–nitrogen mixtures are therefore introduced into outer (or inner) and inner (or outer) flows, respectively. This experimental arrangement allows either the inner flame or the outer flame to be located at different planes by separately adjusting the compositions and injection velocities of the inner and outer flows. An inner (or outer) planar premixed flame with a small outer (or inner) lifted tail or an inner (or outer) nonplanar premixed flame and an outer (or inner) trumpet-shaped diffusion flame can be developed in the flow field. The lifted tail and the trumpet-shaped diffusion flame are stabilized along the interface between the inner and outer jets in the coaxial flow. The inner (or outer) premixed flame influenced by the outer (or inner) oxygen content may experience transports of mass and thermal diffusion parallel to the flame surface. It endures the flow stretch tangent to the flame surface. Furthermore, in the flow field, the directions of flow convection for both inner and outer flows are the same (both divergent). The combustion characteristics, including extinction, blow off, flashback, the transition from the flat flame to the hat-shaped flame, and the ignition and development of diffusion flame are reported and discussed. Finally, the measurements of flame shape and temperature distribution are involved.

Keywords: Flame interaction; Mass transfer; Coaxial flow; Stagnation point

1. Introduction

As a result of the velocity fluctuations and eddy interactions, the flamelets within a turbulent combustion field undergo interactions that are recognized as one of the most important characteristics in the modeling of turbulent combustion. The bulk combustion behaviors such as the extinction characteristics [1,2] as well as the stability of flamelets [3] are significantly modified because of these interactions. Several studies [1–7] have emphasized that interaction of flamelets plays a significant role in real applications of turbulent combustion.

Besides the purely premixed and diffusion flames, flames with intermediate structures called partially premixed flames also occur in turbulent combustion fields [4]. Moreover, flames response to turbulent mixing and the resulting changes in the boundary conditions will usually result in possibilities for interactions of premixed flames, diffusion flames and multiple flames [5]. The gradual transition of burning characteristics from a pure diffusion flame through certain intermediate structures, and finally to premixed flames was initially investigated in counterflow configuration by Lin and Sohrab [6]. Subsequently, characteristics of multiflame burning were

* Corresponding author. Tel.: +886-6-272-4833; fax: +886-6-273-4240.
E-mail address: sshou@mail.ksut.edu.tw (S.-S. Hou).

0017-9310/$ - see front matter © 2003 Elsevier Ltd. All rights reserved.
doi:10.1016/j.ijheatmasstransfer.2003.08.018

further examined through modification of the boundary conditions in counterflows by Hou et al. [7]. The possible burning structures were observed to be single-flame, double-flame and triple-flame burnings in which the individual flame can be burned independently, or burned beyond the flammability limit by the support of another stronger flame [6,7]. An optimum burning identified by the highest values of the maximum temperature and the thickness of the high-temperature zone is achieved under the condition of a triple-flame burning which has a closer approach to the equilibrium combustion state [7].

Studies on interactions of premixed flames and multiple flames introduced above were performed in counterflow configuration in which the interactions are normal to flame surface, and the two interacting premixed flames propagate in opposite directions. In view of chaotic motion of flamelets in turbulent flow, heat and mass transfer parallel to flame surface are also expected to be significant, but have received relatively little attention. To understand the flame interaction induced by unbalanced transport parallel to the flame surface, recently we have conducted an experimental study by using a stagnation-point coaxial flow to develop the nonplanar flame configurations consisting of the inner and the outer flame simultaneously [8]. In the experiment, air and fuel are separately controlled by conventional rotameters, premixed by mixing-loops, and then introduced into the inner and outer flows. The outflowing gases of inner and outer jets, therefore, can impinge on the stagnation plane to generate various flame configurations. The experimental investigation involved measurements and observations of extinction limits, flame configurations and flame-front instability. In addition, we numerically analyzed the transport processes and the fluid mechanics of nonreactive, stagnation-point coaxial flow. Then, the shapes and locations of the flames in combustible stagnation-point coaxial flow were theoretically predicted using a simple model incorporated with the numerical results. The predicted shapes and locations of the flames are in good agreement with the experimental observations.

The importance of parallel flame interactions therefore is clear to us. However, further detailed descriptions on the mechanism of mass and heat transfer for parallel flame interactions are still less known. This paper is a continuation of the preliminary investigation [8]. The objective of the present study is to investigate the characteristics of inner (or outer) premixed flames developed in a stagnation-point coaxial flow under the influence of various outer (or inner) oxygen contents. By using a stagnation-point coaxial flow generated by a lower coaxial burner and an upper quartz plate, an inner (or outer) premixed flame influenced by outer (or inner) oxygen content is experimentally developed to simulate and study double-flame burning structures modified by interactions of flamelets in turbulent combustible flows. The stagnation-point coaxial flow configuration studied herein may closely simulate burning structures influenced by interactions of flames and oxygen concentrations with heat and mass transfer parallel to the flame surfaces. In the experiments, a mixture of fuel and air and a mixture of oxygen and nitrogen are introduced into outer (or inner) and inner (or outer) flows, respectively. We keep the exit velocity of coaxial burner constant, but vary the outer (or inner) fuel concentration and inner (or outer) oxygen concentration. The combustion characteristics, including extinction, blow off, flashback, the transition from a flat flame to a hat-shaped flame, and the ignition and development of diffusion flame are reported and discussed. Furthermore, the measurements of flame shape and temperature distribution are conducted.

2. Experimental

Fig. 1 shows a schematic illustration of the experimental apparatus. The stagnation-point coaxial flow system consists of a quartz plate, 10 mm thick and 110 mm in diameter, which acts as the stagnation plane, and a vertically aligned coaxial burner in which the compositions and injection velocities of the inner and outer flows can be separately controlled. The coaxial burner is composed of an inner copper tube with an inside diameter of 20 mm and an outside diameter of 23 mm, and an outer copper tube with an inside diameter of 49 mm and an outside diameter of 51 mm. The outlet edge of the inner cylindrical tube is sharpened to minimize the flow recirculation (bluff body effect) adjacent to the exit region between the inner and outer jets. A series of small wire-mesh screens and honeycombs are installed inside the tubes to produce uniform velocity distributions at the exit plane of the coaxial burner. The separation distance between the exit plane of the coaxial burner and the quartz plate is adjustable but kept at 13 mm in the experiment.

Oxygen, nitrogen, air and fuel (methane or propane) are separately controlled by conventional rotameters, premixed by mixing-loops, and then introduced into the inner and outer flows. In the experiment, either the inner jet or the outer jet represents an oxidizer jet, which is a mixture of oxygen and nitrogen. $\Omega_{O_2,i}$ and $\Omega_{O_2,o}$ denote the oxygen concentration for the inner jet and the outer jet, respectively. Additionally, a mixture of fuel (methane or propane) and air flowing through either the inner jet or the outer jet indicates a fuel–air premixture jet in which the corresponding inner and outer fuel concentrations are denoted by Ω_i and Ω_o, respectively. The outflowing gases of inner and outer jets then impinge on the stagnation plane to generate various flame configurations through pilot ignition.

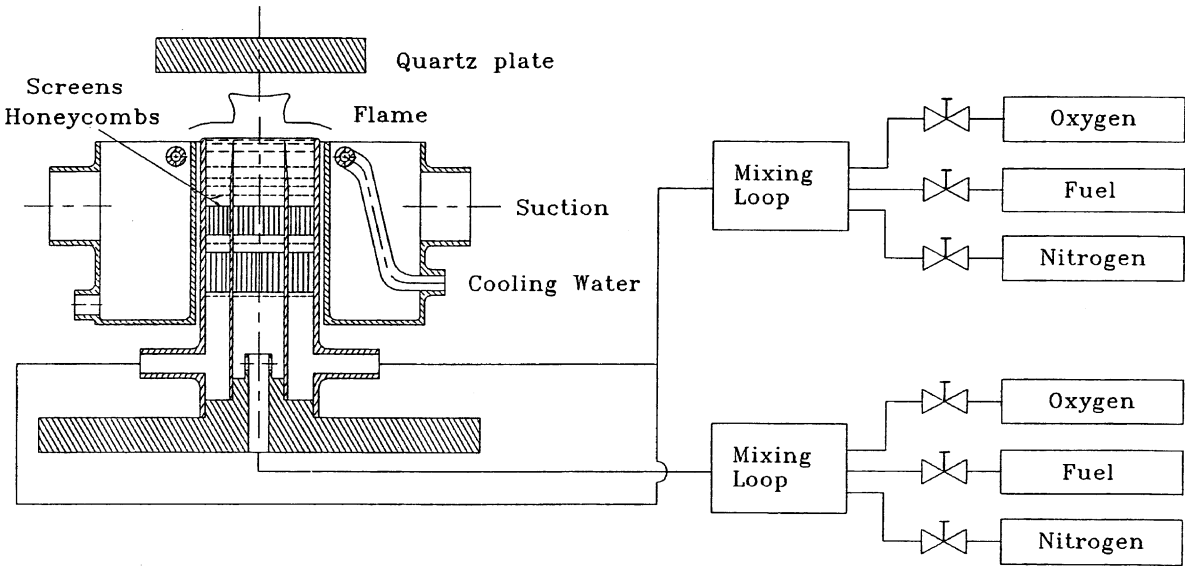

Fig. 1. Schematic diagram of the experimental apparatus.

Furthermore, Fig. 1 shows that the outer tube is equipped with a ring of cooling water similar to that used by Kent and Williams [9], and an exhaust system to remove the combustion products. The exhaust system prevents the heating of the stagnation-plane by otherwise rising combustion products due to buoyancy. Temperature measurements are performed using a silica-coated Pt–Pt–13% Rh thermocouple with 0.075 mm wire diameter. The junction can be traversed both horizontally and vertically by means of a three-dimensional positioner. No correction is made for the radiation loss from the thermocouple in the present study.

This experimental arrangement allows either the inner flame or the outer flame to be located at different axial planes by separately adjusting the compositions and injection velocities of the inner and outer flows. An inner (or outer) planar premixed flame with an outer (or inner) lifted flame tail or an inner (or outer) nonplanar premixed flame and an outer (or inner) trumpet-shaped diffusion flame can be developed in the flow field. The lifted flame tail and the trumpet-shaped diffusion flame are stabilized along the interface between the inner and outer jets in the coaxial flow. The inner (or outer) premixed flame influenced by the outer (or inner) oxygen content may experience radial transports of mass and thermal diffusion parallel to the flame surface, and it also endures the flow stretch tangent to the flame surface. Furthermore, in the flow field, the directions of flow convection for both inner and outer flows are the same (both divergent).

3. Results and discussion

3.1. The influence of outer oxygen concentration on inner flames

In the following experiment, the mixture of fuel and air is introduced into the inner jet, while the mixture of oxygen and nitrogen is introduced into the outer jet. Therefore, the effects of outer oxygen concentration on the inner flame can be investigated. Fig. 2(a) shows the various observed configurations of methane flames as functions of Ω_i and $\Omega_{O_2,o}$ under a fixed injection velocity ($V_o = V_i = 50$ cm/s in the left half; while $V_o = V_i = 60$ cm/s in the right half). Meanwhile, Fig. 2(b) shows the various observed configurations of propane flames as functions of Ω_i and $\Omega_{O_2,o}$ under a fixed injection velocity ($V_o = V_i = 65$ cm/s). Here, V represents the injection velocity at the exit plane of the coaxial burner. The subscripts "o" and "i", respectively, designate the outer flow and the inner flow. Ω_i and $\Omega_{O_2,o}$ denote the fuel concentration for the inner jet and the oxygen concentration for the outer jet, respectively. The coordinate used in the maps, $(\Omega_{O_2,o}, \Omega_i)$, is assigned to indicate the locations of experimental conditions for convenience. The flame shapes sketched in Figs. 2 and 3 consist of thick lines, thin lines, and dotted lines, which represent rich premixed flames (RPF), lean premixed flames (LPF), and diffusion flames (DF), respectively. The definitions of symbols for the curves are as follows. The extinction of inner flat LPF is shown by the horizontal line with "△", and the inner blow off boundary is shown by the horizontal

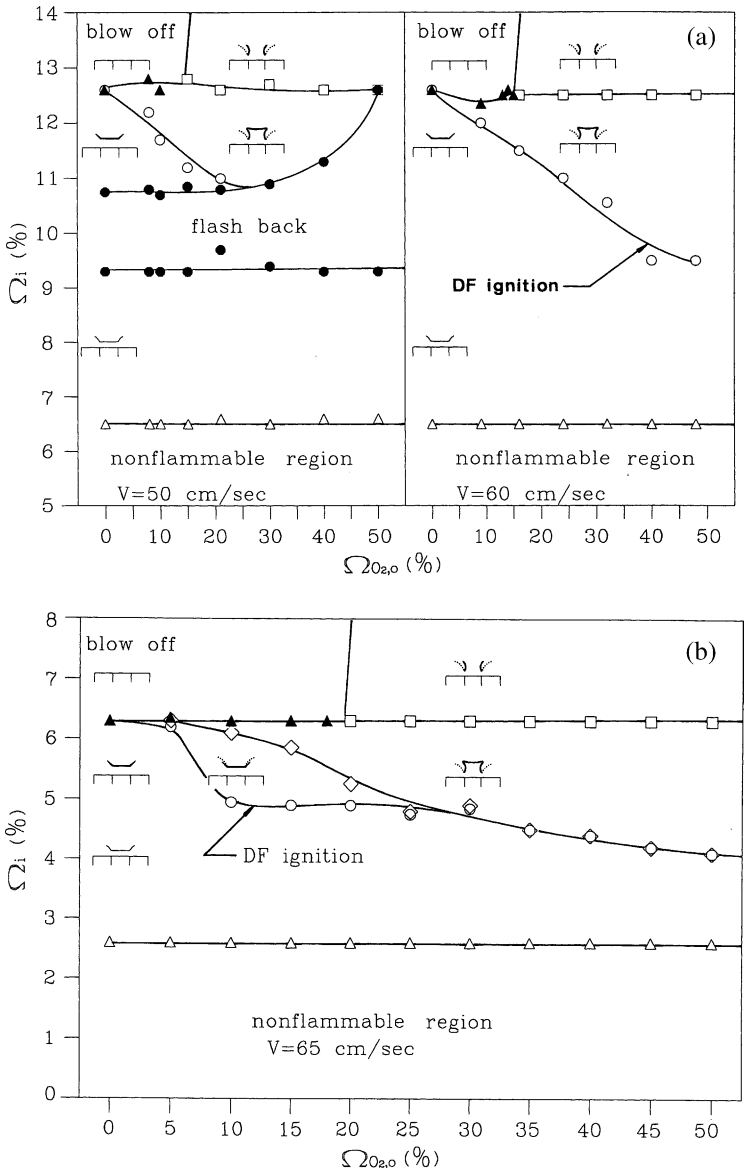

Fig. 2. Combustion characteristics as functions of $\Omega_{O_2,o}$ and Ω_i for (a) methane–air mixtures, (b) propane–air mixtures under a fixed injection velocity.

line with "▲". The transition from the hat-shaped RPF to the trumpet-shaped RPF is identified by the line with "□". The transition from the flat flame to the hat-shaped flame is illustrated by the line with "◇". The initiation of DF is shown by the line with "O". The flashback boundary of inner flame is denoted by the line with "●".

3.1.1. Extinction limits

Fig. 2(a) and (b) demonstrate that the lean limits of the inner methane–air and propane–air mixtures occur at about $\Omega_i = 6.5\%$ and 2.6%, respectively; while the rich limits occur at about $\Omega_i = 12.6\%$ and 6.3%, respectively. Note that the flammable region, identified as the extent between the lean and rich extinction limits, can be significantly modified in the presence of interactions. It is clear that the present limits are narrower than those determined by other methods [10,11] due to the influences of flow stretch and downstream heat loss to the quartz plate. Furthermore, the present lean limits of the inner methane–air and propane–air mixtures are found to be nearly independent of $\Omega_{O_2,o}$ because the inner

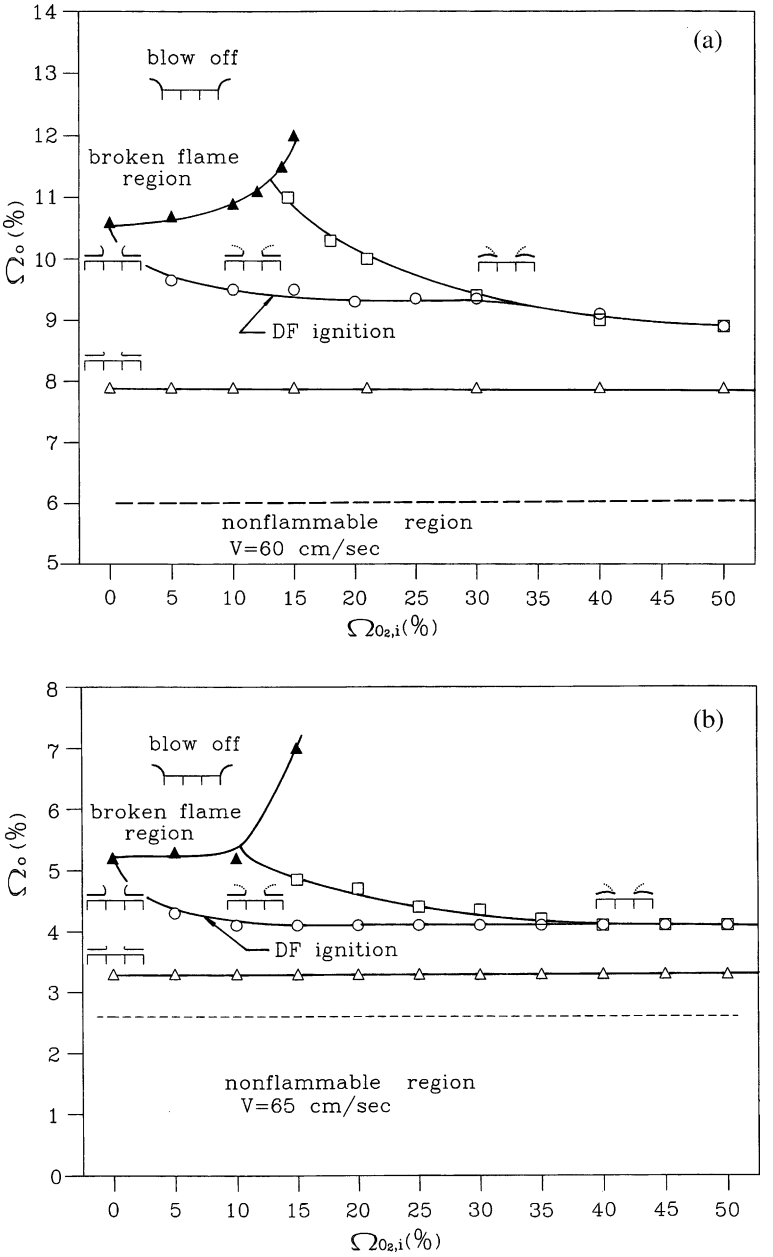

Fig. 3. Combustion characteristics as functions of $\Omega_{O_2,i}$ and Ω_o for (a) methane–air mixtures, (b) propane–air mixtures under a fixed injection velocity.

mixture is so lean that it cannot provide excess fuel to react with the outer oxygen.

3.1.2. Flame transition, double-flame structure and DF ignition

Under the condition of $(\Omega_{O_2,o}, \Omega_i) = (0\%, 7\%)$ in Fig. 2(a), we observe that a planar LPF sits in the inner flow, and it has a small lifted tail near the interface of the inner and outer jets. The small tail is an indication of flow mixing and fuel leakage between the coflowing jets. Starting with the $(\Omega_{O_2,o}, \Omega_i) = (0\%, 7\%)$ condition along the $\Omega_{O_2,o} = 0\%$ line, in which the outer jet is a pure nitrogen jet, as Ω_i is decreased to approach 6.5%, the weakened methane flame with $Le < 1$ sits closer to the wall and experiences a larger flow stretch. Consequently, flame extinction occurs results from the heat loss to the wall when the flame locates near the stagnation-plane [10,12]. However, increasing the Ω_i (under stoichiometric

ratio, 9.5%) along the $\Omega_{O_2,o} = 0\%$ line produces an opposite trend. This means that a strengthened flame is located closer to the burner exit. The increase of Ω_i will lead to flame flashback (denoted by the "●") if the injection velocity is not large enough, as shown in left half of Fig. 2(a). Moreover, by further increasing the value of Ω_i to higher than stoichiometric ratio (approximately 9.5% in this experiment), as shown in the right half of Fig. 2(a), there exists only an inner flat RPF and an outer lifted (trumpet-shaped) flame tail without the occurrence of diffusion flame because the outer jet is a pure nitrogen jet that cannot provide oxygen. Similarly, the lifted flame tail, generated along the interface of the inner and outer jets, is caused by the flow mixing and the fuel leakage between the coflowing jets. The increasing Ω_i ends with the inner blow off boundary shown by the horizontal line with "▲".

In Fig. 2(a), at $(\Omega_{O_2,o}, \Omega_i) = (40\%, 7\%)$, the flame shape is similar to that at $(\Omega_{O_2,o}, \Omega_i) = (0\%, 7\%)$ but the lifted flame tail of the latter is slightly wider than the former. These flame shapes are further displayed in detail in Fig. 4. If $\Omega_{O_2,o}$ is kept constant at 40%, as shown in the right half of Fig. 2(a), a double-flame burning structure composed of a hat-shaped RPF and a trumpet-shaped DF appears when Ω_i is higher than 9.5% but lower than 12.6%. It is found that with increasing the oxygen content in the outer jet, fuel concentration in the inner jet required for the onset of the diffusion flame (identified by the lines with "○") decreases and asymptotically approaches stoichiometric ratio ($\Omega_i = 9.5\%$ for methane–air mixture and $\Omega_i = 4.5\%$ for propane–air mixture). One realizes that a diffusion flame develops when both fuel and oxygen concentrations are sufficient. This asymptotic behavior indicates that no matter how large the oxygen concentration in the outer jet is there is no diffusion flame if the fuel concentration in the inner jet is lower than the stoichiometric ratio. It is interesting to note that the transition from the flat inner flame to the hat-shaped inner flame (denoted by "◇") and the initiation of diffusion flame (denoted by "○") appear simultaneously for the methane–air mixture, as shown in Fig. 2(a). This overlapping phenomenon is also observed in Fig. 2(b) for $\Omega_{O_2,o} > 30\%$ and $\Omega_i < 4.5\%$. While, the propane concentration in the inner jet (or the oxygen concentration in the outer jet) required for the onset of the diffusion flame is smaller than that required for the occurrence of the transition from the flat inner flame to the hat-shaped inner flame for $\Omega_{O_2,o} \leqslant 30\%$ (or $\Omega_i \geqslant 4.5\%$) in Fig. 2(b).

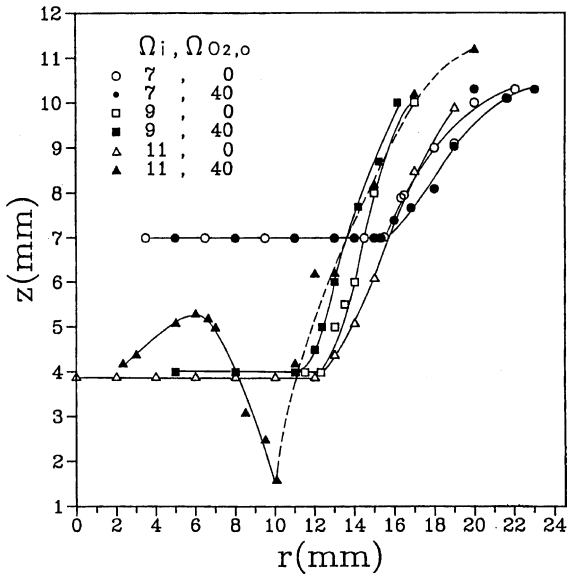

Fig. 4. Flame shapes as functions of $\Omega_{O_2,o}$ and Ω_i for methane–air mixtures ($V = 60$ cm/s).

When the hat-shaped RPF is developed in the inner jet, the continuous increase of Ω_i will gradually weaken the inner RPF, but strengthen the outer DF. Consequently, the transition from a hat-shaped RPF to a trumpet-shaped RPF (denoted by "□"), that is, the extinction of the top of the hat-shaped RPF occurs at about $\Omega_i = 12.6\%$ and 6.3% in Fig. 2(a) and (b), respectively. However, the trumpet-shaped RPF can be burned beyond the extinction limit by the support of another stronger flame (diffusion flame). It is of interest to note that if the values of $\Omega_{O_2,o}$ are higher than 15% and 20% in Fig. 2(a) and (b), respectively, the extinction of the top flame surface of the hat-shaped RPF (denoted by "□") is found to be relatively insensitive to the $\Omega_{O_2,o}$ and the development of the diffusion flame. On the other hand, blow off (a global extinction of the whole flame, denoted by "▲") rather than the extinction of the top part of the hat-shaped RPF occurs if the values of the $\Omega_{O_2,o}$ are lower than 15% and 20% in Fig. 2(a) and (b), respectively.

In the right half of Fig. 2(a), starting with the $(\Omega_{O_2,o}, \Omega_i) = (0\%, 11\%)$ condition along the $\Omega_i = 11\%$ line in which the outer jet is a pure nitrogen jet, the gradual increase of $\Omega_{O_2,o}$ first causes the downstream tail of diffusion flame to generate near the stagnation plane, then the diffusion flame grows gradually downward along the interface of the inner and outer jets, and finally the fully developed diffusion flame stabilizes further upstream and is almost simultaneously accompanied by the transition from the flat flame to the hat-shaped flame. By comparing Fig. 2(a) and (b), combustion characteristics of the latter are similar to those of the former except that by increasing the $\Omega_{O_2,o}$ but keeping Ω_i constant ($\Omega_i > 4.5\%$), first the diffusion flame is initiated, then the transition from flat flame to hat-shaped flame is observed as soon as $\Omega_{O_2,o}$ is large enough. For $\Omega_{O_2,o} \geqslant 30\%$ in Fig. 2(b), the curve of DF ignition coincides with the curve with "◇" showing the transition from the flat flame to the hat-shaped flame.

3.1.3. Flame flashback

Additionally, two types of flashback are identified for $V = 50$ cm/s, as shown in left half of Fig. 2(a). For $\Omega_{O_2,o} \leqslant 25\%$, flashback occurs in the inner jet; while for $\Omega_{O_2,o} > 25\%$, flashback occurs at the interface of inner jet and outer jet. For $\Omega_{O_2,o} > 25\%$, the oxygen concentration is sufficient such that the burning intensity of DF is strong enough. Therefore, the base of the bulk double-flame (RPF and DF) tends to move upstream (downwards) and stabilizes at the location near the burner exit due to the support of DF and the effect of flow mixing. This flame base characteristic provides a good explanation of the phenomenon that flashback occurs at the interface of the inner jet and the outer jet. Furthermore, with increasing $\Omega_{O_2,o}$, the value of Ω_i for the upper limit of flashback is first almost the same, then is promptly increases after $\Omega_{O_2,o} > 30\%$, and finally merges at the inner flame extinction limit (the extinction of the top flame surface of hat-shaped RPF, denoted by "□"). However, the lower limit of flashback shows that the Ω_i at flashback condition is independent of $\Omega_{O_2,o}$; that is, it is almost a constant, 6.3%.

3.2. The influence of inner oxygen concentration on outer flames

Fig. 3(a) and (b) shows the combustion characteristics of the outer flame as functions of Ω_o and $\Omega_{O_2,i}$ under a fixed injection velocity ($V_o = V_i = 60$ cm/s in Fig. 3(a), and $V_o = V_i = 65$ cm/s in Fig. 3(b)) for the methane–air mixture and propane–air mixture, respectively. In this set of experiment, the mixture of fuel and air are introduced into the outer jet, while the mixture of oxygen and nitrogen are introduced into the inner jet. Therefore, the influence of inner oxygen concentration on the outer flame can be examined. In Fig. 3(a) and (b), Ω_o and $\Omega_{O_2,i}$ denote the fuel concentration for the outer jet and the oxygen concentration for the inner jet, respectively.

3.2.1. Extinction limits

The nonflammable boundary is shown by the dashed line and the lean outer flame is locally broken and unstable when Ω_o locates between the dashed line and the horizontal line with "△". The horizontal line with "△", thereby, represents that the lean planar outer flame without the existence of broken flame is stabilized in the given flow field. An additional region for the possible occurrence of the broken flame is also shown by the curve with "▲" for the rich mixture. The Ω_o required for the occurrence of rich broken flame is increased with increasing $\Omega_{O_2,i}$. On the other hand, the Ω_o required for the occurrence of lean broken flame is insensitive to $\Omega_{O_2,i}$. Fig. 3(a) and (b) show that the lean limits of the outer methane–air and propane–air mixtures occur at about $\Omega_i = 7.8\%$ and 3.2%, respectively. The blow off boundary (or rich limit) of the outer flame occurs at $\Omega_o = 12\%$ for methane–air mixture and at 6% for propane–air mixture, respectively.

3.2.2. Flame transition, double-flame structure and DF ignition

In Fig. 3(a) and (b), the line with "○" shows the initiation of DF. The Ω_o required for the onset of diffusion flame decreases with increasing the $\Omega_{O_2,i}$. This phenomenon is similar to that of the inner flame. In Fig. 3(a), at $(\Omega_{O_2,i}, \Omega_o) = (0\%, 10\%)$, namely the outer jet is a pure nitrogen jet, the flame consists of an outer strong planar RPF and an inner flame tail. The establishment of inner weak flame tail in this case is similar to that of the outer one at $(\Omega_{O_2,o}, \Omega_i) = (0\%, 11\%)$ in Fig. 2(a). With enlarging $\Omega_{O_2,o}$, the flame tail becomes longer and stronger. The downstream tail shows the weak diffusion flame generated near the stagnation plane. With further increasing $\Omega_{O_2,o}(\Omega_{O_2,o} \leqslant 20\%)$, the diffusion flame grows downward along the interface of the inner and outer jets, and finally the fully developed trumpet-shaped diffusion flame stabilizes in the flow field. Therefore, the flame composed of a trumpet-shaped DF and a flat LPF is initially established. As the $\Omega_{O_2,o}$ is increased to greater than 20%, the flame base, in which the diffusion flame and the RPF connect, goes further upstream and stabilizes at the location near the burner exit due to the support of DF and the effect of flow mixing. The critical condition for the initiation of the flame base going further upstream is denoted by the curve with square symbols. The $\Omega_{O_2,i}$ required for the onset of the flame base initially concave to the burner exit diminishes and finally approaches asymptotically stoichiometric ratio with increasing $\Omega_{O_2,i}$. The curve of DF ignition coincides with the curve of the flame base initially concave to the burner exit if the $\Omega_{O_2,i}$ is sufficient high ($\Omega_{O_2,i} \fallingdotseq 35\%$ in Fig. 3(a) and $\Omega_{O_2,i} \fallingdotseq 40\%$ in Fig. 3(b)).

3.3. Comparisons of combustion characteristics for inner and outer flames

Table 1 summarizes the comparisons of combustion characteristics for inner and outer flames. In comparing with Fig. 2(a) (or Fig. 2(b)), Fig. 3(a) (or Fig. 3(b)) indicates that the inner flame is easier to be stabilized in the given flow field, that is the inner flame has a wider flammable region, identified by the extent between the lean and rich limits, than the outer flame. The blow off boundary of the outer (or inner) flame occurs at $\Omega_o = 12\%$ (or $\Omega_i = 12.6\%$) for methane–air mixture and at 6% (or $\Omega_i = 6.3\%$) for propane–air mixture, respectively. Additionally, in comparing with Fig. 2(a) (or Fig. 2(b)), Fig. 3(a) (or Fig. 3(b)) shows that a less amount of oxygen concentration ($\Omega_{O_2,i}$) is required for the onset of the diffusion flame as Ω_o is held at a constant (above stoichiometric ratio). It reveals clearly that diffusion flame is easier to be stabilized in the flow field where the

Table 1
Comparisons of combustion characteristics for inner and outer flames in a coaxial flow with a stagnation point

	Inner flame influenced by outer oxygen	Outer flame influenced by inner oxygen
O_2 convection	Outwards	Outwards
O_2 diffusion	Inwards	Outwards
Lean limit	6.5% for CH_4–air	7.8% for CH_4–air
	2.6% for C_3H_8–air	3.2% for C_3H_8–air
Rich limit or blowoff boundary	12.6% for CH_4–air	12.0% for CH_4–air
	6.3% for C_3H_8–air	6.0% for C_3H_8–air
Flammable region	Wider	Narrower
DF ignition	At a higher O_2 concentration	At a lower O_2 concentration

mixture of fuel and air are introduced into the outer jet, while the mixture of oxygen and nitrogen are introduced into the inner jet. In the flow field that is composed of an inner jet of O_2 and N_2 and an outer jet of fuel and air, the directions of flow convection and mass transport of oxygen for inner flow are the same. Therefore, the diffusivity of the oxygen is strongly enhanced under the influence of flow convection. However, the inner flame (examined in Fig. 2(a) and (b)) influenced by outer oxidizer (oxygen and nitrogen) is easier to be stabilized in the given flow field. In other words the inner flame has a wider flammable region, identified by the extent between the lean and rich limits, than the outer flame because the strength of the latter is suppressed by the effects of flow stretch and upstream heat loss to the burner rim.

3.4. Flame profiles

Fig. 4 (or Fig. 5) shows the various methane–air flame profiles for selected inner (or outer) flames influenced by outer (or inner) oxygen concentration. In the figures, "z" and "r" respectively denote the axial and radial coordinates in which the origin is located at the center of the exit plane of the lower coaxial burner. The location of flame surface is defined as the center of the luminous zone. In the absence of outer oxygen ($\Omega_{O_2,o} = 0\%$), i.e., the outer jet is a pure nitrogen jet, the flame consists of an inner planar LPF and an outer trumpet-shaped flame tail for both $(\Omega_{O_2,o}, \Omega_i) = (0\%, 7\%)$ and $(\Omega_{O_2,o}, \Omega_i) = (0\%, 9\%)$. However, for $(\Omega_{O_2,o}, \Omega_i) = (0\%, 11\%)$, it consists of an inner planar RPF and an outer lifted (trumpet-shaped) flame tail. For a fixed exit velocity, $V = 60$ cm/s, as Ω_i (lean condition) is decreased, the weakened inner LPF is pushed closer to the stagnation plane and endures a larger flow stretch. Thus, the axial position (z) of the inner flame at $(\Omega_{O_2,o}, \Omega_i) = (0\%, 7\%)$ is higher than that of the flame at $(\Omega_{O_2,o}, \Omega_i) = (0\%, 9\%)$. Furthermore, the radial position, at which the interface of the LPF and the lifted flame tail locates, shows that $(\Omega_{O_2,o}, \Omega_i) = (0\%, 7\%)$ has a slightly larger value than $(\Omega_{O_2,o}, \Omega_i) = (0\%, 9\%)$ because it endures a larger flow stretch. Therefore, the outer lifted (trumpet-shaped) flame tail of $(\Omega_{O_2,o}, \Omega_i) = (0\%, 7\%)$ is slightly wider than that of $(\Omega_{O_2,o}, \Omega_i) = (0\%, 9\%)$. The axial flame position of the inner planer RPF of $(\Omega_{O_2,o}, \Omega_i) = (0\%, 11\%)$ is slightly higher than that of the inner planar LPF of $(\Omega_{O_2,o}, \Omega_i) = (0\%, 9\%)$.

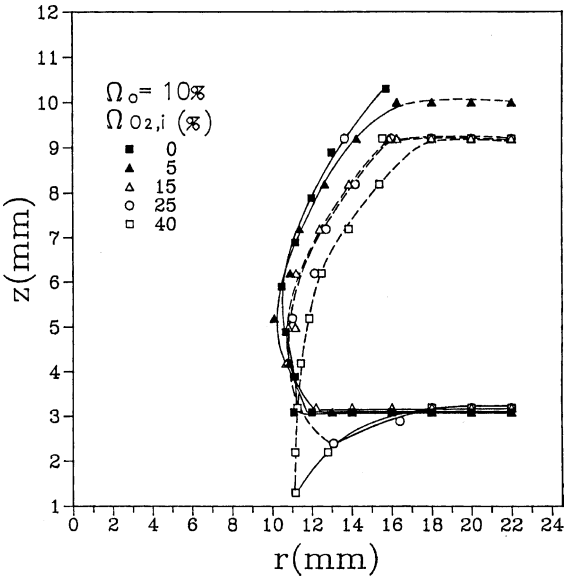

Fig. 5. Flame shapes as functions of $\Omega_{O_2,i}$ and Ω_o for methane–air mixtures ($V = 60$ cm/s).

By increasing the outer oxygen concentration ($\Omega_{O_2,o}$) to 40%, the influence of the $\Omega_{O_2,o}$ on the inner flame profile is examined in Fig. 4. The flame profiles of $(\Omega_{O_2,o}, \Omega_i) = (0\%, 7\%)$ and $(\Omega_{O_2,o}, \Omega_i) = (40\%, 7\%)$ are nearly the same except that the lifted flame tail of the latter is slightly wider than that of the former. Similarly, the flame profiles of $(\Omega_{O_2,o}, \Omega_i) = (0\%, 9\%)$ and $(\Omega_{O_2,o}, \Omega_i) = (40\%, 9\%)$ are almost the same, while the flame tail of the latter is slightly narrower than that of the former since the average molecular weight of the outer jet of the latter is heavier than that of the former. At $(\Omega_{O_2,o}, \Omega_i) = (40\%, 11\%)$, the nonplanar flame consists of an inner hat-shaped RPF (a top part and a rim part) and an outer trumpet-shaped diffusion flame. The center portion of the inner flame surface is slightly

concave when viewed from top. Furthermore, the flame base, at which the hat-shaped RPF and the trumpetshaped DF coincides, moves further upstream and develops near the burner exit. Both the flame base characteristic and the transition from the planar RPF to the hat-shaped RPF have been discussed earlier.

For a fixed Ω_o, 10%, the influence of $\Omega_{O_2,i}$ on the flame profile of outer flame can be further explored in Fig. 5. As $(\Omega_{O_2,i}, \Omega_o) = (0\%, 10\%)$, namely the outer jet is a pure nitrogen jet, the flame consists of an outer strong planar RPF and an inner weak flame tail. With enlarging $\Omega_{O_2,i}$ to be 5% or 15%, the outer RPF is still planar, while the flame tail becomes longer and stronger. The downstream tail denoted by the dashed line with solid-triangle symbols shows the weak diffusion flame that is initially generated near the stagnation plane and gradually developed along the interface of the inner and outer jets. With further increasing the $\Omega_{O_2,i}$ to be 25%, the enhanced diffusion flame grows further downward along the interface of the inner and outer jets, and strengthens the outer RPF to sit closer to the burner exit. Therefore, the flame base, at which the trumpedshaped DF and the nonplanar RPF connect, is basically a circular rim and may move closer to the burner exit. As the $\Omega_{O_2,i}$ is increased to be 40%, the flame base stabilizes much closer to the port of burner due to the support of DF and the effect of flow mixing. Moreover, it is found that the increase in $\Omega_{O_2,i}$ causes the inner trumpet-shaped flame to be more divergent.

3.5. Radial temperature profiles

In this section, we mainly discuss the radial temperature distributions for methane–air mixtures, as shown in the right half of Fig. 2(a). Radial temperature distributions for different cross-sections of the flames at $(\Omega_{O_2,o}, \Omega_i) = (0\%, 7\%)$, (40%, 7%), (0%, 9%), (40%, 9%), (0%, 11%), and (40%, 11%) are shown in Figs. 6–11, respectively. In the experiment, the injection velocity is fixed at $V = 60$ cm/s, and the corresponding flame shapes can be referred to Fig. 4. For the condition of $(\Omega_{O_2,o}, \Omega_i) = (0\%, 7\%)$, the inner flame is located at $z = 7$ mm for $r \leqslant 15$ mm. According to Fig. 6, for $z \leqslant 10$ mm the increase of axial position results in an enlargement of the isothermal high-temperature zone near the central axis because the high temperature region bounded by the inner planar flame and the outer lifted (trumpet-shaped) flame tail is enlarged and has uniform distribution. However, for $z = 11$ mm near the stagnation plane, the decay of the maximum temperature is found due to the effect of downstream heat loss. For a given axial position (z), with increasing radial position (r), the temperature is initially nearly constant, and then gradually decreased when the positions of measurement exceed the position of the outer flame tail. Considering the case of $(\Omega_{O_2,o}, \Omega_i) = (40\%, 7\%)$ shown in Fig. 7, radial

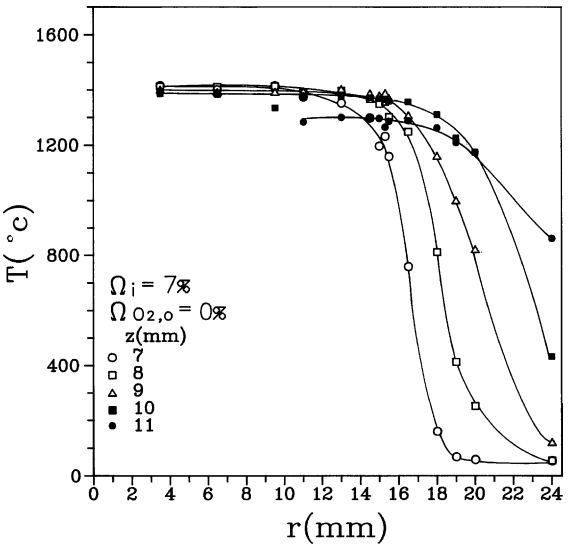

Fig. 6. Radial temperature distributions at various axial positions for methane–air mixtures as $(\Omega_{O_2,o}, \Omega_i) = (0\%, 7\%)$ and $V = 60$ cm/s.

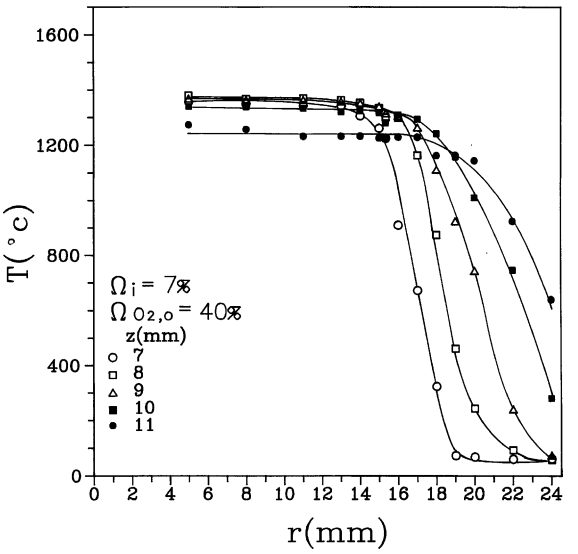

Fig. 7. Radial temperature distributions at various axial positions for methane–air mixtures as $(\Omega_{O_2,o}, \Omega_i) = (40\%, 7\%)$ and $V = 60$ cm/s.

temperature distributions in response to the different cross-sections are similar to those shown in Fig. 6. However, the maximum temperature for $(\Omega_{O_2,o}, \Omega_i) = (40\%, 7\%)$ is slightly lower than that for $(\Omega_{O_2,o}, \Omega_i) = (0\%, 7\%)$.

The inner flame of $(\Omega_{O_2,o}, \Omega_i) = (0\%, 9\%)$, located at $z = 4$ mm for $r \leqslant 11$ mm (as shown in Fig. 4), is stronger than that of $(\Omega_{O_2,o}, \Omega_i) = (0\%, 7\%)$. Therefore,

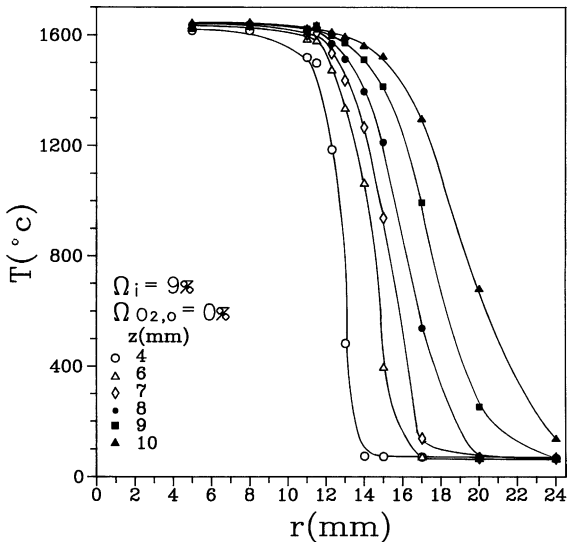

Fig. 8. Radial temperature distributions at various axial positions for methane–air mixtures as $(\Omega_{O_2,o}, \Omega_i) = (0\%, 9\%)$ and $V = 60$ cm/s.

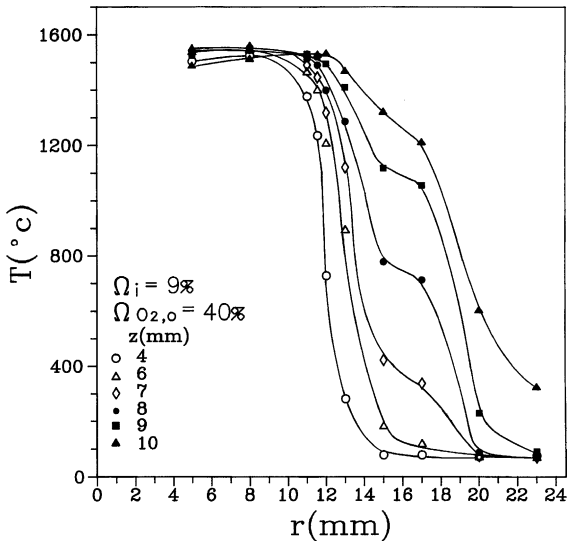

Fig. 9. Radial temperature distributions at various axial positions for methane–air mixtures as $(\Omega_{O_2,o}\Omega_i) = (40\%, 9\%)$ and $V = 60$ cm/s.

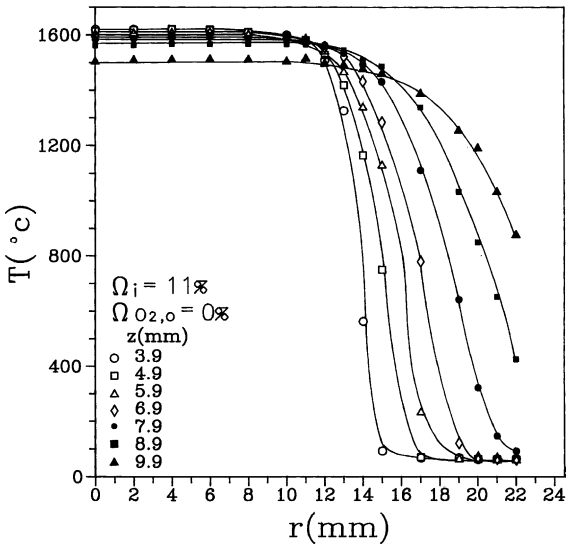

Fig. 10. Radial temperature distributions at various axial positions for methane–air mixtures as $(\Omega_{O_2,o}\Omega_i) = (0\%, 11\%)$ and $V = 60$ cm/s.

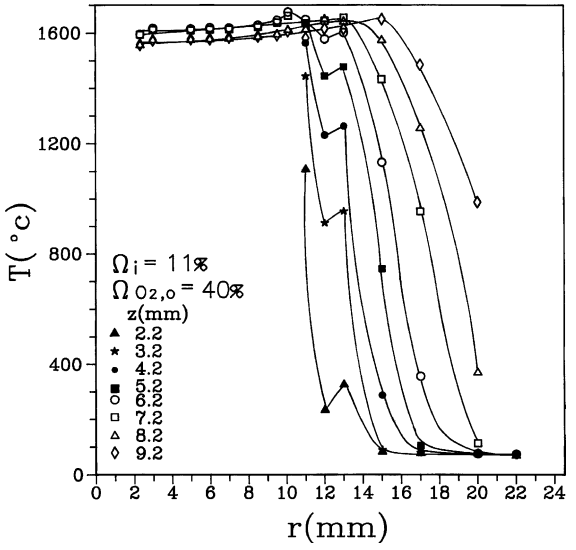

Fig. 11. Radial temperature distributions at various axial positions for methane–air mixtures as $(\Omega_{O_2,o}\Omega_i) = (40\%, 11\%)$ and $V = 60$ cm/s.

the former sits closer to the burner exit and experiences smaller flow stretch than the latter. When compared with Fig. 6, Fig. 8 shows a narrower isothermal high-temperature zone due to the slightly smaller area of the inner planar LPF surface. However, the whole high-temperature region of $(\Omega_{O_2,o}, \Omega_i) = (0\%, 9\%)$, bounded by the inner planar flame and the outer trumpet-typed flame tail, is larger than that of $(\Omega_{O_2,o}, \Omega_i) = (0\%, 7\%)$. Therefore, the high-temperature zone of $(\Omega_{O_2,o}, \Omega_i) = (0\%, 9\%)$ is increased further downstream. Fig. 8 also shows an enlargement of the isothermal high-temperature zone near the central axis as z increases from 4 to 10 mm. In addition, Fig. 8 shows similar combustion characteristics to those in Fig. 6. That is, with increasing

radial position, the temperature is initially nearly constant and then gradually decreases. Radial temperature distributions of $(\Omega_{O_2,o}, \Omega_i) = (40\%, 9\%)$ corresponding to the different cross-sections shown in Fig. 9 are similar to those of $(\Omega_{O_2,o}, \Omega_i) = (0\%, 9\%)$ shown in Fig. 6. However, it is interesting to note that the change of radial temperature gradient (with respect to radial position) takes place abruptly when the position of measurement crosses the surface of lifted flame tail (in the range of 15 mm $\leqq r \leqq$ 17 mm for $z = 7$, 8 and 9 mm). Furthermore, the maximum temperature of $(\Omega_{O_2,o}, \Omega_i) = (40\%, 9\%)$ is slightly lower than that of $(\Omega_{O_2,o}, \Omega_i) = (0\%, 9\%)$.

Fig. 10 shows radial temperature distributions of $(\Omega_{O_2,o}, \Omega_i) = (0\%, 11\%)$ with respect to the different cross-sections. As discussed earlier, the trend is also similar to those of $(\Omega_{O_2,o}, \Omega_i) = (0\%, 9\%)$ and $(\Omega_{O_2,O}, \Omega_i) = (0\%, 7\%)$. The inner flame position of $(\Omega_{O_2,o}, \Omega_i) = (0\%, 11\%)$, located at $z = 3.9$ mm for $r \leqslant 12$ mm (as shown in Fig. 4), is almost the same as that of $(\Omega_{O_2,o}, \Omega_i) = (0\%, 9\%)$. This implies that these two flames possess almost equal burning intensity. Both the isothermal high-temperature, zone and the maximum temperature, therefore, are found to be similar. The radial temperature distributions of $(\Omega_{O_2,o}, \Omega_i) = (40\%, 11\%)$ at different cross-sections shown in Fig. 11 are quite different from those of $(\Omega_{O_2,o}, \Omega_i) = (0\%, 11\%)$ shown in Fig. 10 since the outer diffusion flame of the former has already developed. The top part of the inner RPF has a slightly concave flame surface (when viewed from top) and the trumpet-shaped diffusion flame diffuse heat both inward and outward. Therefore, when the positions of measurement cross the diffusion flame surface, a local temperature jump always occurs (2.2 mm $\leqslant z \leqslant$ 5.2 mm). Furthermore, when compared with the other cases (Figs. 6–10), Fig. 11 represents that in the high-temperature region, bounded by the rim part of the inner hat-shaped RPF and the outer trumpet-typed DF (6.2 mm $\leqslant z \leqslant$ 9.2 mm), the increase of radial position results in a slightly enlarged temperature initially, then the occurrence of maximum temperature at the point near the diffusion flame, and finally the gradual decrease of temperature. This is mainly caused by the strong interaction between the inner RPF and the outer DF.

4. Conclusions

In this study, in order to understand the significant mechanism of heat and mass transport between inner (or outer) oxygen content on outer (or inner) flame, a mixture of oxygen and nitrogen, and fuel and air mixture were introduced into outer (or inner) and inner (or outer) flows, respectively, in a stagnation-point coaxial flow. In the experiment, the exit velocity of coaxial burner was kept constant at all times, while the outer (or inner) fuel concentration and inner (or outer) oxygen concentration were adjustable. In this way, the combustion characteristics, including boundaries for lean- and rich-limit extinction, flashback, the transition from the flat flame to the hat-shaped flame, the ignition and development of diffusion flame and measurements of flame location and temperature distribution were reported and discussed. Results are generally concluded as follows:

(1) The inner flame influenced by outer oxygen content is easier to be stabilized in the given flow field than the outer flame influenced by inner oxygen content. That is, the inner flame has a wider flammable region, identified by the extent between the lean and rich limits, than the outer flame, because the strength of the latter is suppressed by the combined effects of flow stretch and upstream heat loss to the burner rim.

(2) With increasing oxygen content in the outer (or inner) jet, fuel concentration in the inner (or outer) jet required for the onset of diffusion flame decreases and asymptotically approaches the stoichiometric ratio. However, the oxygen diffusivity is strongly enhanced because the directions of oxygen diffusivity and flow convection are both divergent for the case of an outer RPF influenced by inner oxygen concentration. Therefore, a less amount of oxygen concentration is required for the onset of diffusion flame when the outer flame is influenced by inner oxygen content.

(3) When the hat-shaped RPF is developed in the inner jet, the continuous increase of the inner fuel concentration will gradually weaken the inner RPF, but strengthen the outer DF. Consequently, the transition from the hat-shaped RPF to the trumpet-shaped RPF, that is, the extinction of the top of the hat-shaped RPF occurs. Note that the trumpet-shaped RPF can be burned beyond the extinction limit by the support of another stronger flame (diffusion flame).

(4) The transition from the inner flat flame to the inner hat-shaped flame and the initiation of the diffusion flame appear simultaneously for the methane–air mixture. However, for the propane–air mixture the diffusion flame is established first, and then the transition from the flat flame to the hat-shaped flame is observed as soon as the outer oxygen supply is large enough.

(5) The increase in inner oxygen concentration causes the inner trumpet-shaped flame tail to become longer and stronger and to be more divergent. The weak diffusion flame that is initially generated near the stagnation plane and gradually developed along the interface of the inner and outer jets. When the inner oxygen concentration is sufficiently large, the intensified diffusion flame grows further downward along the interface of the inner and outer jets, and strengthens the outer RPF to sit closer to the burner exit.

(6) For the flame composed of an inner planar premixed flame and an outer flame tail, the measurements of radial temperature distribution shows that for a given

axial position (z), as the radial position (r) increases, the temperature is initially kept almost constant, and then gradually decreases when the positions of measurement exceed the position of the outer flame tail. Moreover, the maximum temperature of inner flame influenced by higher outer oxygen concentration (40%) is slightly lower than that of inner flame influenced by zero outer oxygen concentration (0%). However, when the inner hat-shaped RPF, and the outer trumpet-shaped diffusion flame are developed, a local temperature jump always occurs as soon as the positions of temperature measurement cross the diffusion flame surface.

The flow situation is a very complex one, involving phenomena on jet stabilization, jet blow-off, inner-outer jet interaction through mixing and aerodynamics, stagnation flame stabilization, and extinction of stretched flames. In this study, we keep the exit velocity of coaxial burner constant, but vary the outer (or inner) fuel concentration and inner (or outer) oxygen concentration. We realize that the jet velocities are crucial to the stabilization and blowoff process, and consequently the different flame configurations. Therefore, the influences of different and unequal jet velocities on flame phenomena for the coaxial flow with a stagnation point are important and worth further study.

Acknowledgements

This work was supported by the National Science Council, Taiwan, ROC, under Contracts of NSC 82-0401-E-006-184 and NSC 89-2212-E-168-003.

References

[1] S.H. Sohrab, Z.Y. Ye, C.K. Law, An experimental investigation on flame interaction and the existence of negative flame speeds, in: Proceedings of the Twentieth Symposium (International) on Combustion, The Combustion Institute, Pittsburgh, 1984, pp. 1957–1965.

[2] S.H. Sohrab, Z.Y. Ye, C.K. Law, Theory of interactive combustion of counterflow premixed flames, Combust. Sci. Technol. 45 (1986) 27–45.

[3] S.H. Sohrab, B.H. Chao, Influences of burner rim aerodynamics on polyhedral flames and flame stabilization, Combust. Sci. Technol. 38 (1984) 245–265.

[4] N. Peters, Partially premixed diffusion flamelets in non-premixed turbulent combustion, in: Proceedings of the Twentieth Symposium (International) on Combustion, The Combustion Institute, Pittsburgh, 1984, pp. 353–360.

[5] P.A. Libby, F.A. Williams, Structure of laminar flamelets in premixed turbulent flames, Combust. Flame 44 (1982) 287–303.

[6] T.H. Lin, S.H. Sohrab, On the transition of diffusion to premixed flames in conserved systems, Combust. Flame 68 (1987) 73–79.

[7] S.S. Hou, C.K. Chang, T.H. Lin, An experimental investigation on multiflame burning structure in conserved system, Combust. Sci. Technol. 79 (1991) 35–48.

[8] S.S. Hou, S.S. Yang, S.J. Chen, T.H. Lin, Interactions for flames in a coaxial flow with a stagnation point, Combust. Flame 132 (2003) 58–72.

[9] J.H. Kent, F.A. Williams, Extinction of laminar diffusion flames for liquids fuels, in: Proceedings of the Fifteenth Symposium (International) on Combustion, The Combustion Institute, Pittsburgh, 1975, pp. 315–325.

[10] M. Kitano, Y. Otsuka, On flammability limits and flame shapes of counterflow premixed flames, Combust. Sci. Technol. 48 (1986) 257–271.

[11] S. Ishizuka, C.K. Law, An experimental study on extinction and stability of stretched premixed flames, in: Proceedings of the Nineteenth Symposium (International) on Combustion, The Combustion Institute, Pittsburgh, 1982, pp. 327–335.

[12] I. Yamaoka, H. Tsuji, An experimental study of flammability limits using counterflow flames, in: Proceedings of the Seventeenth Symposium on Combustion, The Combustion Institute, Pittsburgh, 1979, pp. 843–855.